Effects of rings on flow and temperature in lime kilns

PATRICK GAREAU, MARKUS BUSSMANN, NIKOLAI DEMARTINI, AND HONGHI TRAN

ABSTRACT: A steady state, two-dimensional (2D) axisymmetric model has been developed to help understand how rings form and grow in a typical lime kiln. Rings of varying length, thickness, and geometry at the front and back faces were modeled to study the effects on flue gas flow and temperature.

The results show that ring growth causes the gas velocity to increase and insulates the adjacent refractory, resulting in a lower kiln shell temperature. The results also reveal the formation of recirculation zones immediately downstream of the rings, as well as temperature deviations upstream and downstream of the rings that might promote recarbonation and further ring growth. The model was applied to a kiln from a kraft mill with front-end and mid-kiln rings and good agreement was obtained between the measured and predicted kiln shell temperatures, providing confidence in the modeling.

Application: A lime kiln model has been developed to predict how gas flow and kiln temperatures respond to the presence of ring deposits and may provide insights into how rings form and grow.

Ring formation is a common problem in lime kiln operation. Rings can impact the ability of lime kilns to operate continuously and meet mill demands for lime recovery. Ideally, a kiln will operate for at least a year between shutdowns for maintenance. However, in extreme cases, rapid ring formation can lead to a costly unplanned shutdown in less than a month from a clean start. Moreover, rings can have undesired effects related to gas flow, temperature, combustion, dusting, product quality, and production capacity [1,2].

Rings can form in the cold end of the kiln (often called mud rings); middle of the kiln (mid-kiln rings); and in the hot end (front-end rings). Several factors are known to promote ringing in the different regions of a lime kiln, including high soda and high moisture content in the lime mud feed, the burning of high sulfur-containing fuels, poor flame characteristics, low feed-end temperatures, and unstable kiln operation [2]. Of these, high soda content and unstable kiln operations are often considered the most important [1].

Mid-kiln ring formation is thought to begin with particle adhesion on the exposed refractory surface, which makes a soft lime (calcium oxide; CaO) layer that subsequently becomes hard upon reacting with carbon dioxide (CO_2) in the flue gas [1]. Ring hardening through recarbonation of lime ($CaO + CO_2 \rightarrow CaCO_3$) is known to occur when temperatures drop to below ~800°C. The high sodium content in the lime mud promotes the adhesion of particles to the kiln wall, since sodium compounds, mainly sodium carbonate (Na_2CO_3) and sodium sulfate (Na_2SO_4), melt at around 800°C. Temperature fluctuations in the kiln can then cause the adhered lime to recarbonate and form a harder deposit that is not easily eroded by the tumbling motion of the bed, leading to the initial formation of a stable ring. Each newly adhered layer will insulate the existing layer, driving the recarbonation reaction and promoting further ring growth.

Despite this earlier research, ring growth is still not fully understood, because it is difficult to examine ring formation and measure local conditions in an operating kiln. Simulations are a more practical option for studying local conditions. Computational fluid dynamics (CFD) can be used to model and predict gas flow and heat transfer within a kiln. It has been used extensively over the years for improving the design and operation of rotary kilns with promising results (e.g., [3,4]), although it has never been used to study the effects of rings.

In this work, we use CFD to predict flue gas flow and temperatures inside lime kilns with rings as a function of ring length and thickness, ring location, and ring geometry at the front and back faces. The computational methodology is presented first, followed by the model validation against shell temperature measurements of an actual kiln, and finally results are given on the effect of the various ring geometry parameters.

COMPUTATIONAL METHODOLOGY

A steady state, two-dimensional (2D) axisymmetric lime kiln and ring model has been developed to characterize a typical kiln. The trademarked commercial CFD software ANSYS Fluent (Ansys; Canonsburg, PA, USA) was used to run the simulations. The realizable k-ε model, a non-premixed combustion model, and a discrete ordinates model were used to model turbulence, combustion, and radiation,

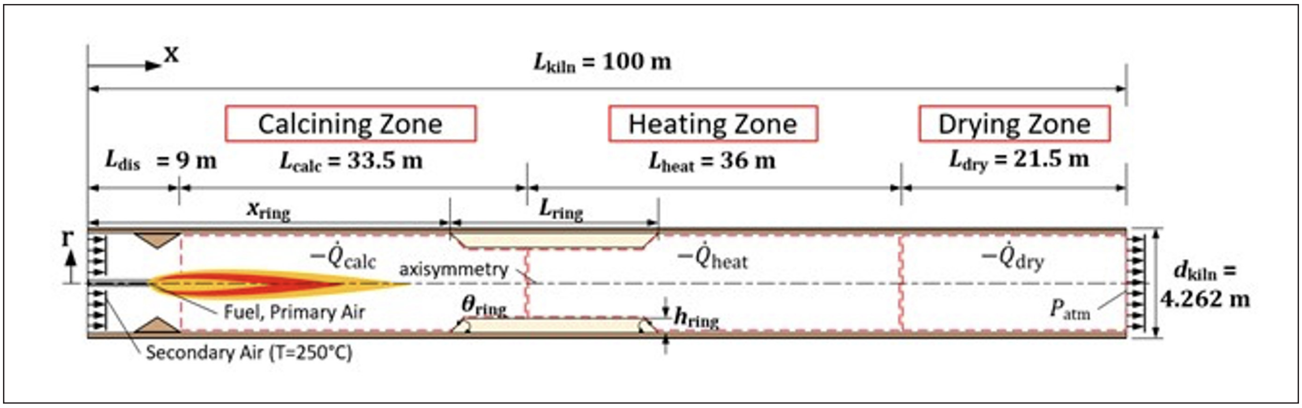

1. Model geometry and boundary conditions.

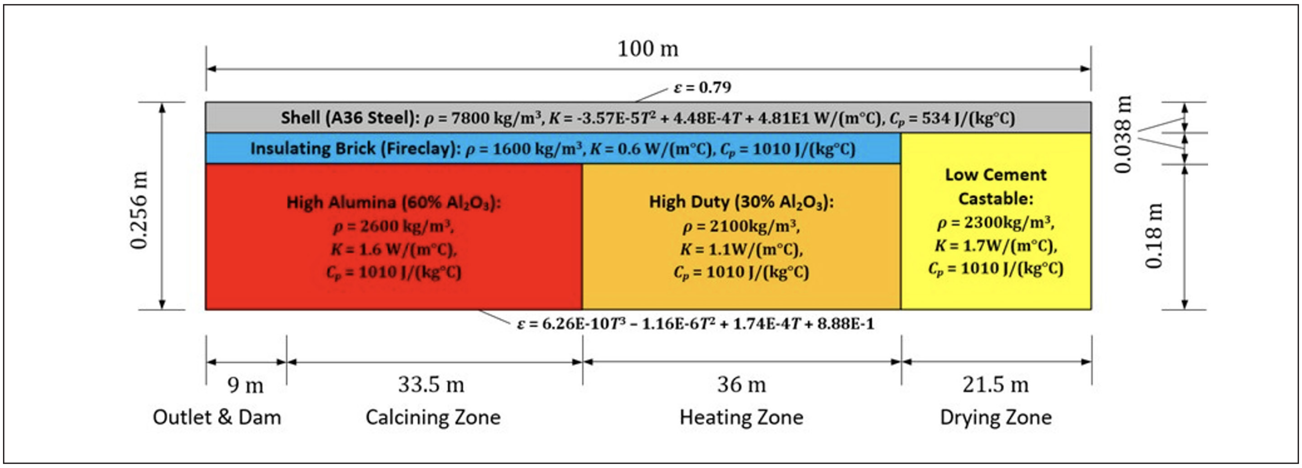

2. Model refractory and shell configuration.

respectively. The bed geometry and flow are not modeled due to the 2D axisymmetric geometry, although a bed heat sink model was developed to account for the drying, heating, and calcining of lime. A simple model was developed to describe ring composition based solely on temperature. Since rings grow relatively slowly, any part of the ring above/below the recarbonation temperature, 800°C, is assumed to be calcium oxide/calcium carbonate ($CaO/CaCO_3$), respectively, which in turn affects the density and thermal conductivity of the ring. The governing equations are discretized in Fluent with the PRESTO! (PREssure STaggering Option) scheme for pressure and second order upwinding for all other equations. A pressure-based solver and coupled pressure-velocity coupling scheme were used to solve the equations. See [5] for detailed solver theory.

The geometry and boundary conditions of the modeled kiln are shown in **Fig. 1**. A concentric methane (CH_4) burner is assumed for simplicity, with separate inlets for fuel, primary air, and heated secondary air. Although the bed is not modeled, a discharge dam is present to account for its effects on gas flow. The kiln interior is divided into four zones where drying, heating, calcining, and discharging of the bed take place; the lengths of these zones were determined based on values in literature [6]. The bed heat sink model prescribes average heat losses in each of the first three zones (approximately 7.63, 5.56, and 15.33 MW, respectively), based on kiln operating conditions and a global conservation of energy analysis. Although the total heat losses are assumed constant in each simulation, their distribution changes due to the rings. The geometry of a ring is described by the four variables illustrated in Fig. 1: ring starting position, x_{ring}; ring length, L_{ring}; ring thickness, h_{ring}; and the geometry of the ring front and back faces, as characterized by the angle, θ_{ring}. Ring thickness was varied from 25.1 to 93.8 cm (corresponding to reductions of cross-sectional area of 25% to 75%). The geometry at the front and back of a ring was varied by considering angles from 15° to 75°. The combined heat loss by mixed convection and radiation to the surroundings was modeled by imposing thermal boundary conditions on the shell exterior.

The simplified double brick refractory and shell configuration is illustrated in **Fig. 2**, and is based on a typical layout given in [6]. The operating conditions of the modeled kiln are listed in **Table I**.

The following material properties were assumed for the ring: for density, ρ_{CaO} = 1512 kg/m³, ρ_{CaCO_3} = 2700 kg/m³; for specific heat capacity, $C_{p,CaO} = C_{p,CaCO_3}$ = 1000 J/(kg°C); for thermal conductivity, K_{CaO} = 3.46E-7T² -1.00E-3T +1.48

Operating Conditions	
Capacity	350 metric tons of CaO/day
Fuel type	CH_4
Excess O_2	2.9%
Primary air ratio	15%
Mean gas outlet temperature	275 ± 10°C
CaO = calcium oxide; CH_4 = methane; O_2 = oxygen.	

I. Modeled kiln operating conditions.

W/(m°C) [7], $K_{CaCO_3} = 0.33 + 672.36/(301+T)$ W/(m°C) [7]; and for emissivity, $\varepsilon_{CaO} = \varepsilon_{CaCO_3}$ = 5.45E-7T^2 -1.18E-3T +1.01 [8]. Additional geometry, boundary conditions, and other modeling details can be found in [9].

RESULTS AND DISCUSSION

Model validation

Figure 3 shows results of a model validation, comparing predicted kiln shell temperatures to those of a kiln at a kraft mill operated by one of the companies that supported this research [10]. The real shell temperature data was measured with an infrared scanner prior to shutdown of the kiln for ring removal. The kiln has a length of approximately 100 m, outer diameter of 3.3 m, and lime capacity of 236 metric tons/day.

The geometry of the mid-kiln ring was approximated based on available sketches by the mill. No information on the smaller front-end ring was available, and so it was not modeled. Overall, the agreement between the predicted and measured kiln shell temperatures is very good. For the most part, the predicted shell temperatures are within 25°C, 35°C, and 40°C of the measured values in the calcining, heating, and drying zones, respectively. Where the unmodeled front-end ring is situated, the shell temperature is overpredicted by ~45°C. Along the mid-kiln ring, the shell temperature is somewhat underpredicted. There could be several reasons for this, including the simplified ring modeling, ring geometry approximation, assumed material properties, thermal boundary conditions imposed, and 2D axisymmetric limitations. Despite the modeling simplifications, the trends in temperature are reasonably well captured, the shell temperature is overall well predicted, and as a result, the model was considered validated.

Effect of ring thickness

To assess the impact of ring geometry and location on gas flow and heat transfer, rings were characterized by prescribing the four variables shown earlier in Fig. 1; namely, the ring starting position, x_{ring}; ring length, L_{ring}; ring thickness, h_{ring}; and the geometry of the ring front and back faces, as characterized by the angle, θ_{ring}. In this section, the effect of thickness of a mid-kiln ring is studied. It is assumed that the mid-kiln ring starts at a location 35 m from the front end (x_{ring} = 35 m) and has a length L_{ring} = 20 m. The θ_{ring} is set to 45°. The ring thickness, h_{ring}, is varied between 25.1, 54.9, and 93.8 cm, corresponding to kiln interior cross-sectional area reductions (A.R.) of 25%, 50%, and 75%, respectively.

Streamline plots of gas flow through the three mid-kiln ring cases are shown in **Fig. 4**. Up until the location where the ring starts, the gas flow is largely unaffected; streamlines are smooth and horizontal, and velocity profiles are practically identical. However, as the gas flow enters the opening of the ring, it converges and speeds up as the area decreases. At the exit of the ring, flow separation occurs. The gas flow exits the ring opening in an expanding jet

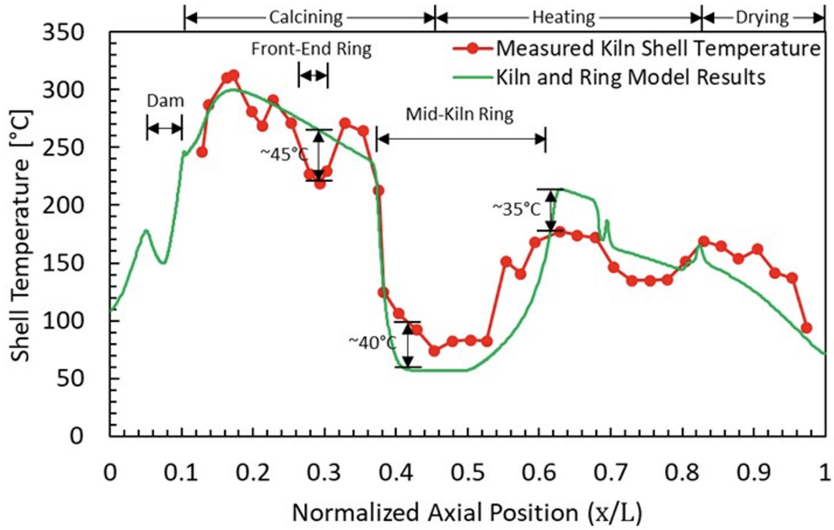

3. Measured kiln shell temperature versus kiln and ring model results.

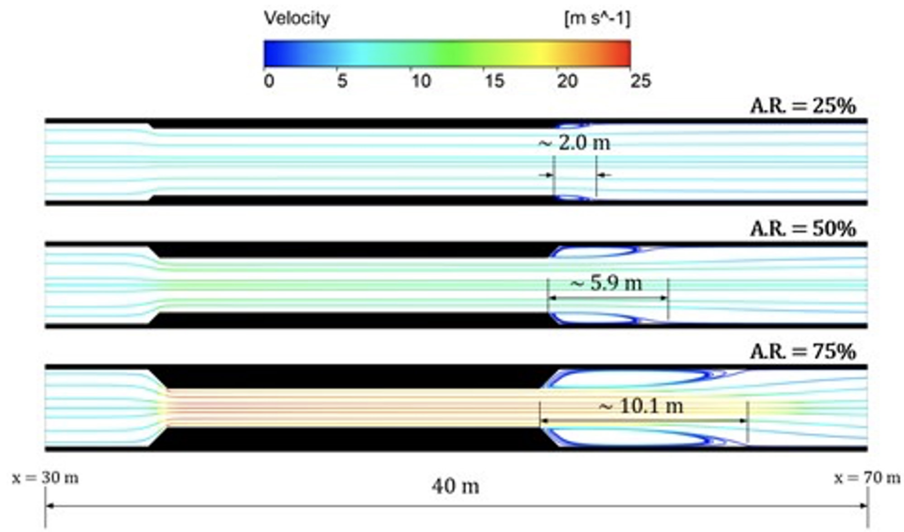

4. Streamline plots of flow through mid-kiln rings of increasing thickness. A.R. is the cross-sectional area reduction.

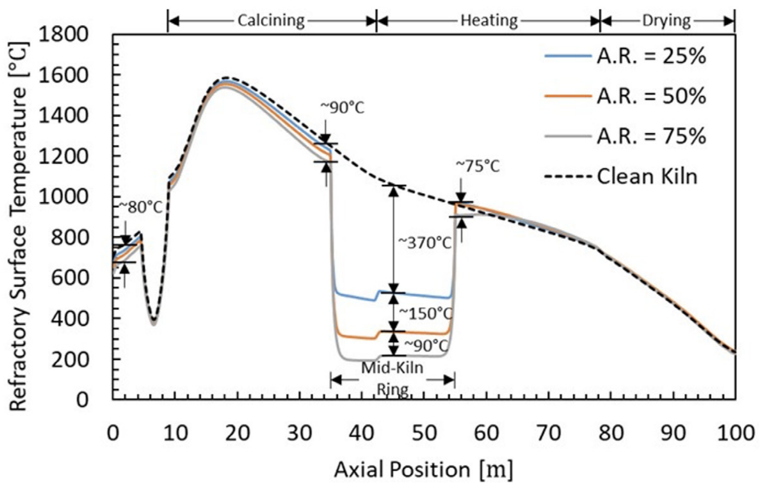

5. Refractory surface temperature changes with increasing mid-kiln ring thickness.

stream, while recirculation zones are formed adjacent to the ring and exposed refractory surface. These recirculation zones are about as thick as the ring and increase in length with increasing ring thickness: for A.R. = 25%, 50%, and 75%, the recirculation zones span ~2.0, 5.9, and 10.1 m, respectively. Overall, the acceleration of the gas flow may affect dust levels in the kiln, because higher velocity flow is more likely to entrain more dust particles from the bed.

The temperature profiles of the refractory surface (i.e., the interface between the refractory and flue gas/ring) for a clean kiln and each of the three mid-kiln ring cases are shown in **Fig. 5**. For the clean kiln case, the temperature reaches a peak in the calcining zone approximately where the flame ends, and then decreases with distance from the burner at a roughly steady rate in each of the calcining, heating, and drying zones. Apart from where the ring is located, similar trends are observed for the three other cases. Upstream of the ring, the refractory surface temperature decreases with increasing ring thickness; this effect is most prominent at locations adjacent to the ring and in the kiln discharge region, where temperatures vary by ~90°C and ~80°C, respectively. By contrast, downstream of the ring, about 65 m from the lime discharge, the refractory surface temperature increases with increasing ring thickness, although to a much lesser degree. Directly adjacent to the ring, temperatures vary by ~75°C, and the thickest ring case yields the lowest local temperature. This can be explained by the recirculation zones that form as the gas flow exits the ring, which have a direct impact on the local convective heat transfer. When comparing the upstream

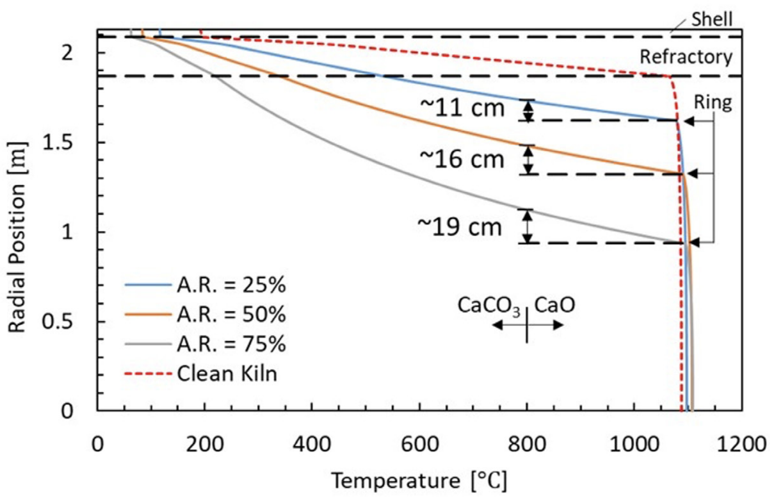

6. Radial temperature profile from the kiln centerline to the shell, as a function of mid-kiln ring thickness. The axial position is at the midpoint of the mid-kiln ring (x = 45 m).

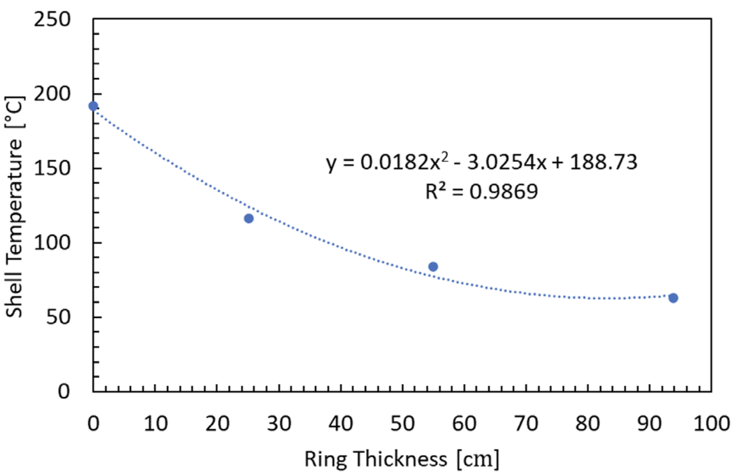

7. Shell temperature plotted against mid-kiln ring thickness. The axial position is at the midpoint of the mid-kiln ring (x = 45 m). The dashed line and equation shown are for a second-order polynomial fit.

and downstream effects on refractory surface temperature, it seems that ring growth is more likely to occur upstream where temperatures tend to decrease, and recarbonation would thus be promoted. Finally, the most prominent temperature variations occur along the lengths of the rings due to insulation effects. Interestingly, the temperature of the refractory surface decreases less with increasing ring thickness. For example, with each incremental area reduction, the changes in temperature at the midpoint of the rings are ~370°C, 150°C, and 90°C, respectively, despite the ring thickness roughly doubling each time. This is due to the strong insulating effect of the ring, which should be accounted for when correlating changes in shell temperature to ring thickness.

These insulation effects are shown more clearly in **Fig. 6**, where radial temperature profiles are plotted at the midpoint of the mid-kiln ring. The refractory, shell, ring, and gas boundaries are indicated. As can be seen, the surfaces exposed to the gas all have similar temperatures, but within the ring, refractory, and shell, temperatures decrease with increasing ring thickness at any given radial position. As was shown earlier, the refractory surface temperature drops to a lesser degree with each increase in ring thickness. The same is true at any radial position, including the shell exterior. Thus, an initial small ring will cause a relatively large drop in shell temperature, whereas each additional increment of area reduction brought on by ring growth will result in relatively smaller drops in temperature. This result has important implications on using shell temperature monitoring to assess ring growth. To illustrate, **Fig. 7** shows the shell temperature plotted against mid-kiln ring thickness and a second-order polynomial fit with good

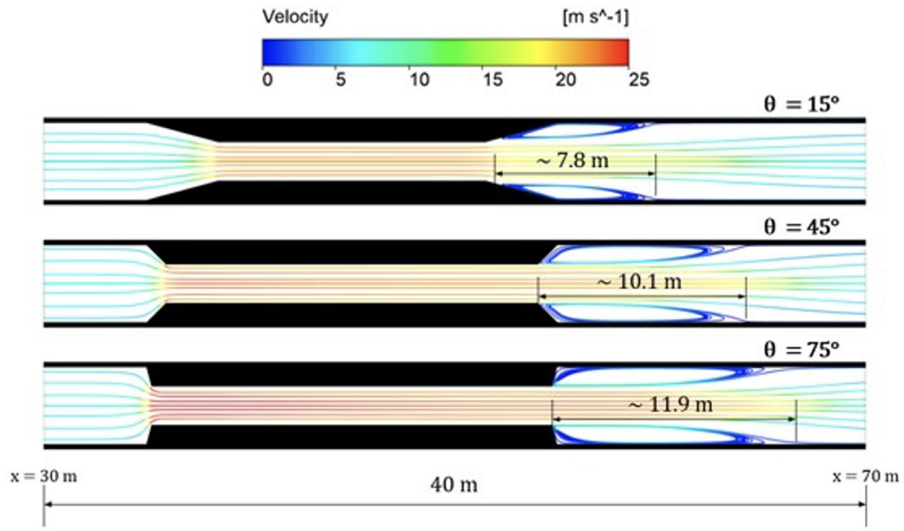

8. Streamline plots of flow through mid-kiln rings of varying front and back face angles.

agreement. The same methodology can be used to construct a similar profile for estimating ring thickness in other kilns.

The recarbonation front position in each ring is also marked in Fig. 6 and corresponds to the distance from the surface of each ring to where the temperature is 800°C (i.e., the point at which CaO transitions to $CaCO_3$). Note that the distance to the recarbonation front equal to ~11, 16, and 19 cm for the A.R. = 25%, 50%, and 75% cases, respectively, varies little with increasing ring thickness. However, the ratio of recarbonated $CaCO_3$ to CaO (on a per-area basis) increases with increasing ring thickness; the ratios are 58%, 74%, and 85% for the A.R. = 25%, 50%, and 75% cases, respectively. This means that the composition of the ring contains increasingly more recarbonated $CaCO_3$ as it grows, making it harder.

Effect of the geometry of the front and back faces of the ring

As the temperatures just upstream and downstream of a ring are a strong function of ring thickness, as shown in Fig. 5, here we consider the effect of varying the ring front and back faces, as characterized by the angle θ_{ring}. A mid-kiln ring with x_{ring} = 35 m, L_{ring} = 20 m, and h_{ring} = 93.8 cm (A.R. = 75%) is assumed, while θ_{ring} is varied between 15°, 45°, and 75°. A thick ring was chosen to accentuate the difference between the three cases. Streamline plots of flow through the three cases are shown in **Fig. 8**. The flow is still largely unaffected upstream of the ring, and very similar jet and recirculation phenomena occur in all three cases. However, as θ_{ring} increases, the flow converges and accelerates more quickly, as expected, and slightly higher velocities are attained in the ring channel. Downstream of the ring, the jet stream expands more slowly and the recirculation zone length increases with increasing θ_{ring}. Recirculation zone lengths are ~7.8, 10.1, and 11.9 m for θ_{ring} = 15°, 45°, and 75°, respectively.

The refractory surface temperatures for these cases and for a clean kiln are shown in **Fig. 9**. Differences in refractory surface temperature are negligible upstream of the ring and along the ring, except at the front and back faces. Downstream of the ring, the effect of the back face angle on flow and temperature is unclear. Immediately downstream of the rings, the refractory surface temperatures vary by ~90°C for the three cases. Temperatures relative to the clean kiln case decrease when θ_{ring} = 45° and 75°, but increase for the θ_{ring}= 15° case. Yet further downstream, the temperatures are all higher than those of the clean kiln, although the refractory surface temperature of the 45° case approaches that of the clean kiln significantly sooner than those of the other two cases. Overall, the effects of varying the front and back faces on temperature are relatively small, especially upstream of the ring.

Effect of ring location

Front-end, mid-kiln, and mud rings are studied in this section. It is assumed that: front-end rings have x_{ring} = 10 m and L_{ring} = 8 m; mid-kiln rings still have x_{ring} = 35 m and L_{ring} = 20 m; and mud rings have x_{ring} = 70 m and L_{ring} = 8.5 m. In each case, θ_{ring} = 45° and h_{ring} = 54.9 cm (A.R. = 50%). Streamline plots of flow through the three ring types are shown in **Fig. 10**.

As in previous cases, the gas flow converges and accelerates as it passes through the ring. In each case, the gas flow exits the ring as an expanding jet stream, forming a recirculation zone adjacent to the ring and refractory surface. The flow through and downstream of the mid-kiln and mud rings are very similar (e.g., the recirculation zone

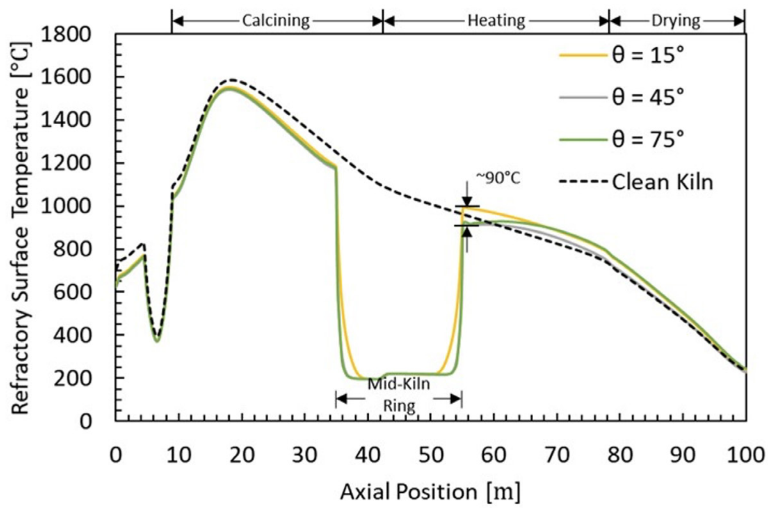

9. Gas-side refractory surface temperature profiles for mid-kiln rings with varying front and back face angles.

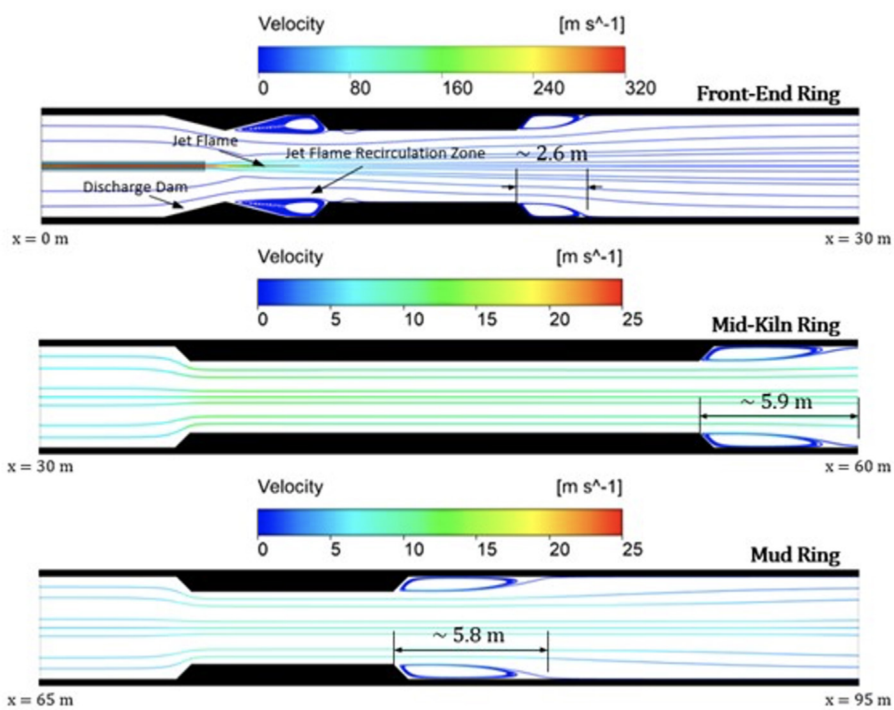

10. Streamline plots of flow through front-end, mid-kiln, and mud rings.

lengths are 5.8 m and 5.9 m), because the upstream flow conditions are very similar for both rings, as they are located far downstream of the burner.

On the other hand, due to the proximity to the burner, front-end rings can have a direct impact on the upstream jet flame recirculation zones, which helps to shape and stabilize the flame. As a result, the jet flame recirculation zone is approximately half its normal length. Front-end rings are therefore much more likely to affect burner operation and result in unsteady flames. Downstream of the front-end ring, the jet expansion and recirculation zones still occur, although they are much shorter; for example, the length of the recirculation zone is only ~2.6 m, which is less than half that of the other two rings. Therefore, downstream of a front-end ring, flow recovers from the disturbance caused by the ring in a shorter distance. Note that the local gas temperature impacts the local gas density and velocity, and therefore the recirculation zones to a certain degree.

The refractory surface temperature for each of the three ring types and for a clean kiln is shown in **Fig. 11**. The

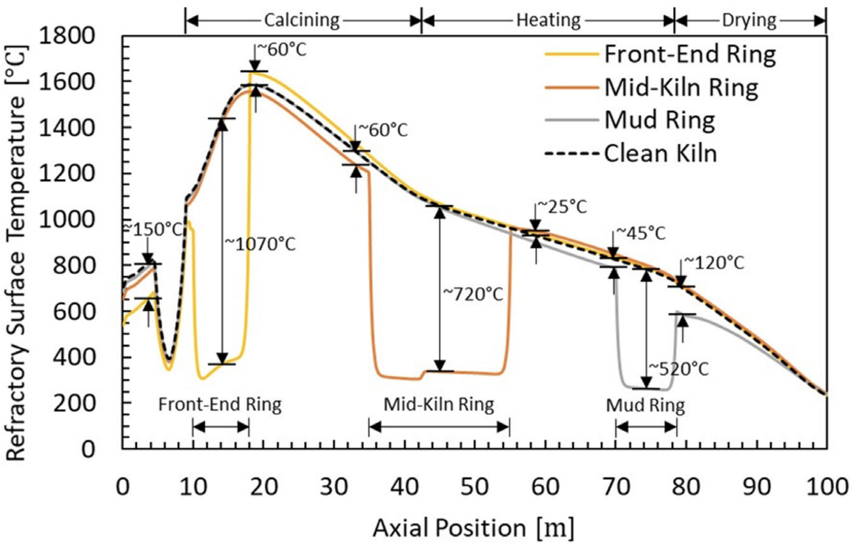

11. Gas-side refractory surface temperature profiles for front-end, mid-kiln, and mud rings.

refractory surface temperature decreases upstream of each ring. It decreases by a similar amount for the mid-kiln and mud ring, ~60°C and ~45°C, respectively, whereas it decreases significantly more for the front-end ring, ~150°C in the discharge region. Downstream of the front-end and mid-kiln rings, the temperatures increase by ~60°C and ~25°C, whereas downstream of the mud ring, the temperature decreases by ~120°C. Once more, the most prominent drop in refractory surface temperature occurs along the span of each ring due to insulation effects. Although the three rings share the same thickness, the temperature drops are different, primarily due to the different local gas temperatures and refractory bricks. For the front-end, mid-kiln, and mud rings, the temperature drops at the mid-section of each ring are ~1070°C, 720°C, and 520°C, respectively. Thus, ring location affects the extent to which the refractory and shell are insulated, which will affect how one uses shell temperature measurements to estimate ring thickness.

CONCLUSIONS

A steady state, 2D axisymmetric lime kiln model has been developed to assess the effect of ringing on gas flow and heat transfer. Rings are characterized by their position within the kiln, length, thickness, and geometry of the front and back faces. Prominent effects of the rings are the increase in gas velocity caused by the reduction in cross-sectional area of the kiln and the insulation of the refractories and shell. For a mid-kiln ring, the change in the location of the recarbonation front is relatively small in the axial direction, but larger in the radial direction, indicating that the thermal driving force for recarbonation increases as the ring grows, which can promote ring hardening. Moreover, the results show that ring growth results in increasingly smaller changes in shell temperature, which must be accounted for by mills using measured shell temperature to estimate ring growth.

Another finding is that gas recirculation zones always form downstream of a ring. These recirculation zones can become long (over 10 m). Their length is affected more by ring thickness than by the face angle at the end of the ring. The formation of these recirculation zones in turn impacts the refractory surface temperature immediately downstream of the ring; hotter temperatures are observed for the front-end and mid-kiln rings, whereas cooler temperatures are observed for the mud ring. The formation of these recirculation zones supports the idea that significant amounts of lime could be carried from the bed at the front of a ring, because of the higher gas velocities that result, and deposited behind the ring, causing further recarbonation and ring growth. Finally, front-end rings can disrupt the upstream jet recirculation zone and destabilize the flame, which in turn can result in undesirable temperature fluctuations in the kiln. **TJ**

ACKNOWLEDGEMENTS

This work is part of the industrial research consortium project Effective Energy and Chemical Recovery in Pulp and Paper Mills - III at the University of Toronto supported by Andritz, Arauco, Babcock & Wilcox, Canadian Kraft Paper, Cenibra, Clyde Bergemann, CMPC, FITNIR, FPInnovations, Georgia Pacific, International Paper, Irving, KFS, Klabin, Mercer, Rayonier, Sappi, Södra, Stora Enso, Suzano, Valmet, and WestRock. We would also like to acknowledge the support of the Natural Sciences and Engineering Research Council of Canada (NSERC), [IRCPJ 517715 -16]. Cette recherche a été financée par le Conseil de recherches en sciences naturelles et en génie du Canada (CRSNG), [IRCPJ 517715 -16].

LITERATURE CITED

1. Tran, H., Mao, X., and Barham, D., *J. Pulp Pap. Sci.* 19(4): J167(1993).
2. Tran, H. and Barham, D., *Tappi J.* 74(1): 131(1991).
3. Elattar, H., Stanev, R., Specht, E., et al., *Comput. Fluids* 102: 62(2014). https://doi.org/10.1016/j.compfluid.2014.05.033.
4. Georgallis, M., Nowak, P., Salcudean, M., et al., *Can. J. Chem. Eng.* 83: 212(2005). https://doi.org/10.1002/cjce.5450830208.
5. ANSYS, "Chapter 21: Solver theory," in *ANSYS® Fluent, 19.1, Help System, Theory Guide*, Ansys Inc., 2019, pp. 679–740.
6. Gorog, J.P., "Selection of refractory bricks for use in lime sludge kilns," *Corrosion in the Pulp and Paper Industry and Biorefineries*, Georgia Institute of Technology, Atlanta, 2014.
7. Silva, M., "Experimental investigation of the thermophysical properties of new and representative materials from room temperature up to 1300°C," Ph.D. thesis, Otto von Guericke University Magdeburg, Madeburg, Germany, 2009.
8. Sandaka, G., "Calcination behavior of lumpy limestones from different origins," Ph.D. thesis, Otto von Guericke University Magdeburg, Madeburg, Germany, 2016.
9. Gareau, P., "A CFD study of the effects of rings on flow and temperature in lime kilns," MASc thesis, University of Toronto, Toronto, Canada, 2020.
10. Keim, E., Zuñiga, J., and Tran, H., *TAPPI J.* 19(7): 345(2020). https://doi.org/10.32964/TJ19.7.345.

ABOUT THIS PAPER

Cite this article as:
Gareau, P., Bussmann, M., DeMartini, N., et al., *TAPPI J.* 21(6): 301(2022). https://doi.org/10.32964/TJ21.6.301

DOI: https://doi.org/10.32964/TJ21.6.301

ISSN: 0734-1415

Publisher: TAPPI Press

About this journal

ABOUT THE AUTHORS

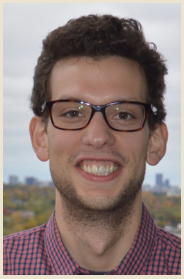

Gareau

Bussmann

DeMartini

Tran

Ring formation is a common problem in lime kiln operation that can impact the ability of lime kilns to operate continuously and meet mill demands for lime recovery. A lime kiln model was developed to predict how gas flow and kiln temperatures respond to the presence of ring deposits, which may provide insights into how rings form and grow.

Accurate modeling was the most difficult aspect of this research. It was addressed by validating the modeled kiln shell temperature profile against that of a kiln from industry, and good agreement was obtained.

We discovered that ring growth causes the gas velocity to increase and the kiln shell temperature to decrease due to insulation. The formation of recirculation zones immediately downstream of the rings, as well as temperature deviations upstream and downstream of the rings, that might promote recarbonation and further ring growth, were also discovered. Moreover, the thermal driving force for recarbonation increases as a mid-kiln ring grows, which can promote ring hardening.

The results show that ring growth results in increasingly smaller changes in shell temperature, which must be accounted for by mills using measured shell temperature to estimate ring growth. Mills can use the introduced model for modeling their kilns.

Possible next steps in this study are further model development to add phenomena currently not taken into account, such as dusting or a fully three-dimensional (3D) model with bed flow, and transient studies.

Gareau is an MASc graduate and Bussmann is professor and chair of the Department of Mechanical & Industrial Engineering at the University of Toronto, Toronto, ON, Canada. DeMartini is assistant professor and Tran is professor emeritus in the Department of Chemical Engineering & Applied Chemistry at the University of Toronto. Email Bussmann at markus.bussmann@utoronto.ca.